NANO LETTERS

Letter

pubs.acs.org/NanoLett

Anisotropic Third-Order Optical Nonlinearity of a single ZnO Micro/Nanowire

Kai Wang,[†] Jun Zhou,*[,†] Longyan Yuan,[†] Yuting Tao,[‡] Jian Chen,[‡] Peixiang Lu,*[,†] and Zhong Lin Wang*[,†,§]

[†]Wuhan National Laboratory for Optoelectronics (WNLO), Huazhong University of Science and Technology (HUST), Wuhan 430074, People's Republic of China

[‡]Instrumental Analysis and Research Center, Sun Yat-sen University, Guangzhou 510275, People's Republic of China

[§]School of Materials Science and Engineering, Georgia Institute of Technology, Atlanta, Georgia 30332-0245, United States

Supporting Information

ABSTRACT: We report a systematic study about the anisotropic third-order optical nonlinearity of a single ZnO micro/nanowire by using the Z-scan method with a femtosecond laser. The two-photon absorption coefficient and nonlinear refraction index, which are measured as a function of polarization angle and sample orientation angle, exhibit oscillation curves with a period of $\pi/2$, indicating a highly polarized optical nonlinearity of the ZnO micro/nanowire. Further studies show that the polarized optical nonlinearity of the ZnO micro/nanowire is highly size-dependent. The results indicate that ZnO nanowire has great potential in applications of nanolasers, all-optical switching and polarization-sensitive photodetectors.

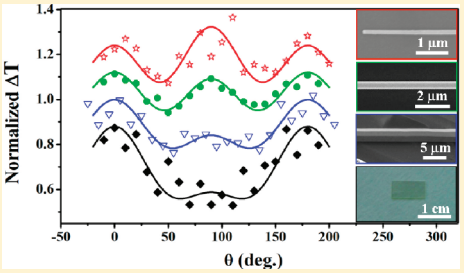

KEYWORDS: *ZnO micro/nanowire, optical nonlinearity, polarization, size-dependent*

In recent years, the nonlinear optical properties of nanomaterials, such as second- and third-harmonic generation (SHG and THG, respectively) effects and two-photon absorption (TPA) effect,[1−14] have attracted much interest due to their potential applications in high-speed information processing,[1−5] nanolasers,[6] optical limiters,[7] and all-optical switching.[8,9] In particular, there has been great interest in the TPA effect of the nanomaterials because of their advantage in imaging[10,11] and nanolaser pumping.[6,12−14] For example, a nanolaser pumped by TPA effect can eliminate the problem of separating the pumping and emission light in single-photon pumping.[15] According to many previous works, the nonlinear optical properties, such as TPA effect is highly dependent on the polarization of the incident laser and the orientation of the sample because of the anisotropy of the semiconductor crystals.[16−21]

ZnO nanowires, a direct wide band gap (3.37 eV) semiconductor with a large excitation binding energy (60 meV), have attracted a wide range of interest both in science and technology.[22−24] Since ZnO nanowire is considered as an important building block for fabricating various nanodevices, it is important to study the anisotropy of the third-order susceptibility, $\chi^{(3)}$, including TPA coefficient and nonlinear refraction (NLR) index of the ZnO nanowire. There are a few reports on the study of polarization effect of the SHG of ZnO films,[18] SHG and THG of the ZnO nanowire,[25] and Raman effect of the ZnO nanorod.[26] From the view of two-photon pumped nanolaser, it is important to systematically study the polarization dependent optical nonlinearities of the ZnO nanowires in order to achieve a high TPA coefficient and a pumping efficiency. However, to the best of our knowledge the information of the anisotropy of TPA coefficient and NLR index of the individual ZnO nanowire in the near-infrared region has been rarely studied.

In this Letter, we report a systematic study on the polarization-dependent third-order nonlinearities (TPA and NLR) of an individual ZnO micro/nanowire in the near-infrared region using the Z-scan method with a femtosecond laser (800 nm, 50 fs). The TPA and NLR as a function of the polarization angle exhibit oscillation curves with a period of $\pi/2$, indicating significant anisotropies of $\chi^{(3)}$ of the individual ZnO micro/nanowire. The size-dependent polarized optical nonlinearities of the ZnO micro/nanowire have also been studied.

Figure 1 shows a schematic the experimental setup for the measurements. The Z-scan method is used to determine the anisotropy of $\chi^{(3)}$ by measuring the transmittance of the sample through an aperture in the far field as a function of the sample position with respect to the focal point (Figure 1a).[17,27] The NLR index (n_2) and the nonlinear absorption coefficient (β) can be measured with (closed aperture, CA) and without the aperture (open aperture, OA), respectively. The femtosecond laser system consisted of a mode-locked Ti/Sapphire oscillator and a regenerative amplifier (Spitfire, Spectra-Physics, 800 nm, 50 fs, 1 kHz) was used as the light source, which was focused by a lens with a focal length of 200 mm. The radius of the beam waist ω_0 was measured to be ~30 μm and then the Rayleigh length, $z_0 = \pi\omega_0^2/\lambda$, was calculated to be 3.5 mm,

Received: November 4, 2011

   dx.doi.org/10.1021/nl203884j | *Nano Lett.* XXXX, XXX, XXX−XXX

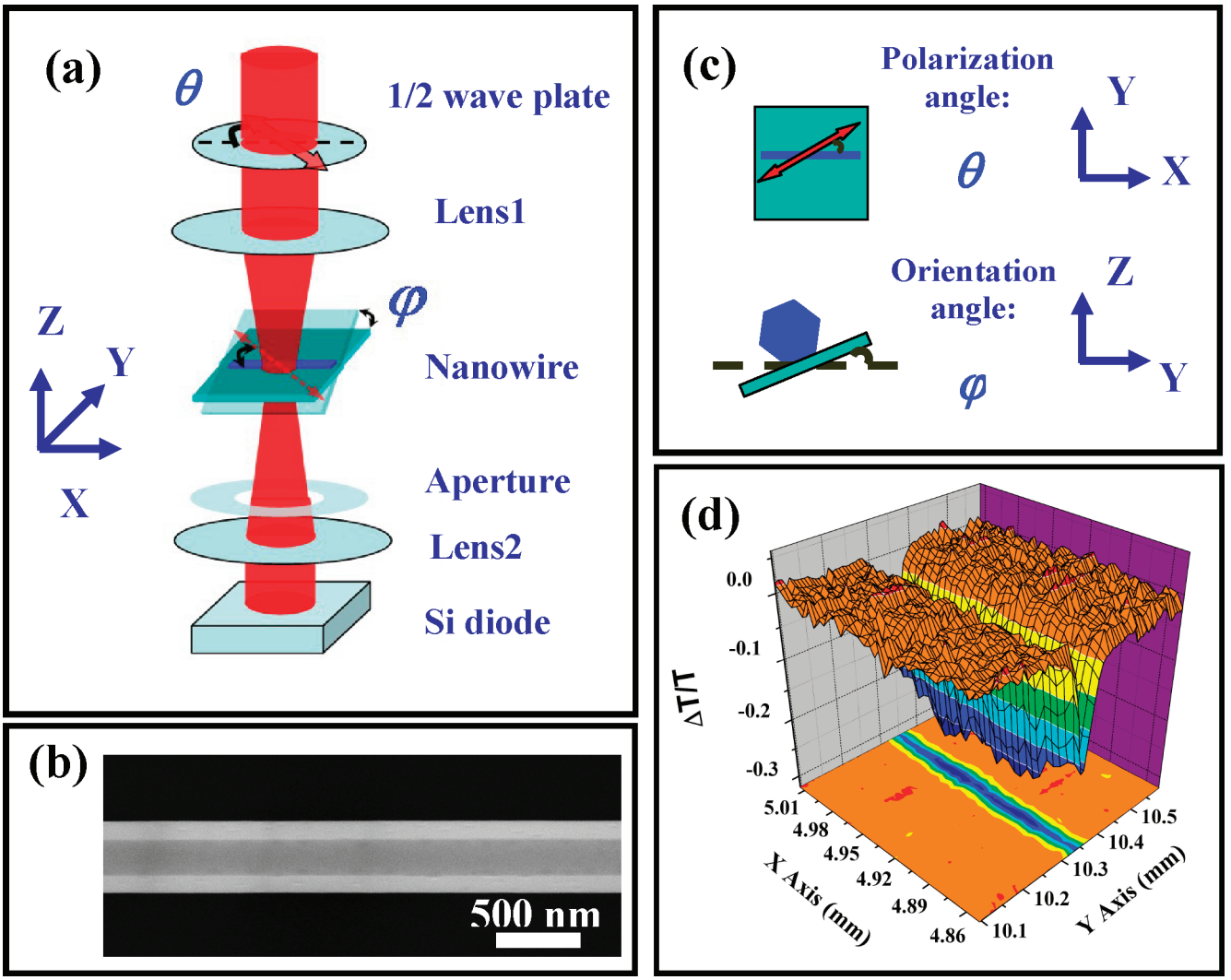

Figure 1. (a) Experimental schemes of the anisotropy nonlinearity measurement. (b) High-magnification SEM image of an ultralong ZnO nanowire on the quartz substrate. (c) The definitions for the polarization angle, θ, and the sample orientation angle, φ. (d) The *XY*-scan pattern of the normalized change of the transmittance, $\Delta T/T$, in a small area of the focal plane ($400 \times 200\ \mu m^2$). The single ZnO microwire with a diameter of 2.6 μm on the substrate is scanned in the focal plane under an excitation intensity of 10 GW/cm^2.

which was much larger than the thickness of the quartz substrate (0.2 mm). Under a low excitation intensity, the nonlinear optical effect of the quartz substrate can be neglected and the large nonlinear effects observed in experiment are attributed to the ZnO micro/nanowire.[17] The transmitted beam through OA or CA was received by a silicon diode (PC20-6, Silicon Sensor GmbH) and double-phase lock-in amplifier (SR830, Stanford Research System).

The ZnO micro/nanowire used for our experiments were synthesized by a high-temperature thermal evaporation process.[22] For optical measurements, single ZnO micro/nanowire was placed on a quartz substrate by using a probe station under optical microscopy.[28−31] Figure 1b shows the high-magnification SEM images of a typical ultralong ZnO nanowire on a quartz substrate which has a hexagonal cross section with a diameter of ~500 nm. As the ZnO exhibits a hexagonal structure, we can conclude that the growth direction of the ZnO nanowire is along *c*-axis. The Raman spectrum of the single ZnO nanowire was conducted under unpolarized backscattering geometry with Raman shift ranging from 200 to 700 cm^{-1} (see Supporting Information, Figure S1). The main Raman features of E_2 (High) at 439.3 cm^{-1} is observed, and a second-order Raman feature of $2E_2$(M) is also observed at 333.3 cm^{-1}, which can be attributed to the undoped ZnO.[32]

In Figure 1c, the *c*-axis of the ZnO micro/nanowire was placed along the *X*-axis, the polarized angle with respect to the *c*-axis, θ, is defined, which is controlled by rotating a half wave plate. The angle between *Y*-axis and the substrate is defined as the sample orientation angle, φ, which controls the incidence plane of the ZnO micro/nanowire. It sets to be 0° as the substrate is perpendicular to *Z*-axis. As it is shown in Figure 1d, an *XY* stage (MVP-25XA, Newport) was used to give a two-dimensional scan that the normalized change of the transmittance, $\Delta T/T$, has been measured in a small area of the focal plane ($400 \times 200\ \mu m^2$)[33]

$$\frac{\Delta T}{T} = \frac{\Delta P}{P} = \frac{P_t - P_i}{P_i} \quad (1)$$

where P_i and P_t are the incident and the transmitted powers. It exhibits a pattern with a long length (*X*-axis) of several-hundred micrometers but a much narrow width (*Y*-axis). Because of the negligible nonlinear absorption of the quartz substrate, this wirelike signal observed can only be attributed to the

dx.doi.org/10.1021/nl203884j | Nano Lett. XXXX, XXX, XXX−XXX

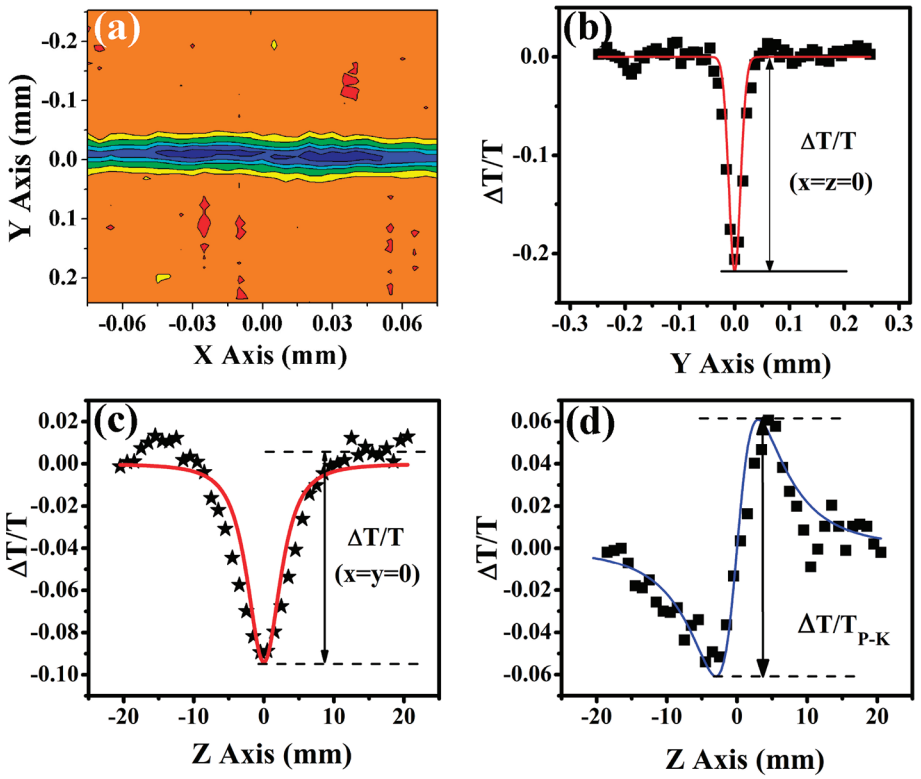

Figure 2. (a) The wirelike 2D pattern of $\Delta T/T$ in functions of X and Y axes in focal plane with a long length and a much shorter width. (b,c) The typical scan curves of the $\Delta T/T$ as a function of Y-axis at $z = x = 0$ and Z-axis at $x = y = 0$, respectively. (d) The CA/OA Z-scan data at $\varphi = 0°$. The solid line indicates the theoretical fit.

ZnO micro/nanowire. Furthermore, the value of $\Delta T/T$ decreases as the excitation intensity increases, indicating a nonlinear absorption process of the ZnO micro/nanowire (see Supporting Information, Figure S2).

In Figure 2a, it exhibits a two-dimensional pattern of XY-scan of the ZnO microwire with a diameter of 2.6 um, while a curve of $\Delta T/T$ as a function of Y-axis in the focal plane ($x = z = 0$) is shown in Figure 2b. The single microwire can be positioned at the center of the focal spot, where the largest $|\Delta T/T|$ can be obtained. For the sample that is much smaller than the spot size of the beam (nanoparticle or nanowire), the transmitted power can be written as[34]

$$P_t = P_i - q(r, z)I(r, z) \tag{2}$$

where $q(r, z) = \beta I(r, z)L_{eff}$, β is the nonlinear absorption coefficient and L_{eff} is the effect sample length. The value of the $\Delta T/T$ as a function of Y-axis in the focal plane and the Z-axis can be written as

$$\frac{\Delta T}{T}(y, \theta) = -\frac{\beta(\theta)I_0L_{eff}}{\sqrt{\pi}\left(\frac{\omega_0}{\Delta y}\right)} \exp\left[-4\left(\frac{y}{\omega_0}\right)^2\right] \tag{3}$$

$$\frac{\Delta T}{T}(z, \theta) = -\frac{\beta(\theta)I_0L_{eff}}{\sqrt{\pi}\left(\frac{\omega_0}{\Delta y}\right)\left(1 + \left(\frac{z}{z_0}\right)^2\right)^{3/2}} \tag{4}$$

where the intensity at the center of the beam at the focus ($z = 0$), I_0, is calculated to be about 3 GW/cm^2. Δy is the width of the ZnO micro/nanowire. The curves of Y-scan ($x = z = 0$), as well as Z-scan ($x = y = 0$) shown in Figure 2b,c can be fitted well by using eqs 3 and 4, respectively. Thus, the TPA coefficient as a function of polarized angle, $\beta(\theta)$, is in proportion to the absolute value of $\Delta T/T$ at $x = y = z = 0$. In Figure 2d, it shows the typical CA/OA results at $\varphi = 0°$, which is related to the NLR properties of the ZnO micro/nanowire. The value of the normalized difference of the extreme transmitted powers (peak and valley) ΔP_{P-V} can be used to determine the on-axis ($x = y = 0$) relative change of the value nonlinear refraction index (n_2) as a function of the polarized angle (θ).[27]

The amplitude of the third-order nonlinear polarization vector can be presented as follows[17]

$$P^{(3)}(\omega) = \frac{3\varepsilon_0}{4}\chi^{(3)}_{eff}(\omega)E^3 \tag{5}$$

where ε_0 is the dielectric permittivity and $\chi^{(3)}_{eff}$ is the effective third-order susceptibility whose functional form depends on the symmetry and orientation of the sample. Figure 3a shows the $|\Delta T/T|$ as a function of the sample orientation angle φ at $\theta = 0°$. Since θ keeps as a constant and the polarization direction is along the c-axis, only one tensor component, $\chi^{(3)}_{zzzz}$, is excited. The increase of $|\Delta T/T|$ at $\varphi = 30°$ from $|\Delta T/T|$ at $\varphi = 0°$ is attributed to the increase of the thickness of the ZnO micro/nanowire. In Figure 3b, it shows $|\Delta T/T|$ versus the sample orientation angle φ at $\theta = 90°$. The low vibration data indicates that no obvious polarized anisotropy can be observed. In this situation, wave vector $\mathbf{k}$ is normal to the c-axis, the electric-field polarization is relative to $[10\bar{1}0]$ crystallographic axis in the crystal graphic xy plane. The intrinsic permutation symmetry leaves only three independent tensor components given by $\chi^{(3)}_{xxxx}$, $\chi^{(3)}_{xyyx}$, and $\chi^{(3)}_{xxyy}$. For this specific geometry, the effect third-order susceptibility

dx.doi.org/10.1021/nl203884j | Nano Lett. XXXX, XXX, XXX−XXX

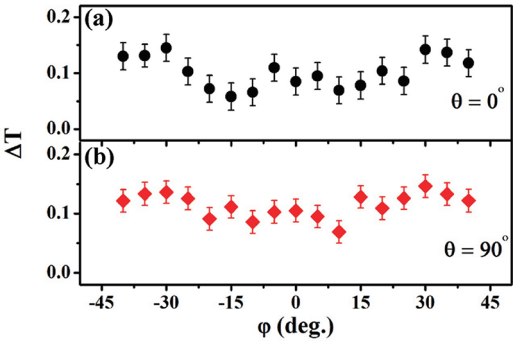

Figure 3. The absolute value of the normalized change in transmittance, $\Delta T/T$, as function of the sample orientation angle, φ, with the polarization angle, θ, kept as a constant of (a) 0° and (b) 90°, respectively.

from eq 5 is

$$\chi^{(3)}_{\text{eff}}(\phi) = \chi^{(3)}_{xxxx}[1 + 2\sigma(\sin^4\phi - \sin^2\phi)] \quad (6)$$

where a coefficient of anisotropy, σ, is defined as

$$\sigma = \frac{\chi^{(3)}_{xxxx} - [\chi^{(3)}_{xxyy} + 2\chi^{(3)}_{xyyx}]}{\chi^{(3)}_{xxxx}} \quad (7)$$

Because of the isotropy in the xy plane and $\chi^{(3)}_{xxxx} = \chi^{(3)}_{xxyy} + 2\chi^{(3)}_{xyyx}$, the coefficient of anisotropy is zero. Thus, $\chi^{(3)}_{\text{eff}}$ is equal to $\chi^{(3)}_{xxxx}$.

Figure 4a,b show $|\Delta T/T|$ and $|\Delta T/T|_{\text{p-v}}$ as a function of the polarization angle θ at $\varphi = 0°$. The electric-field polarization in

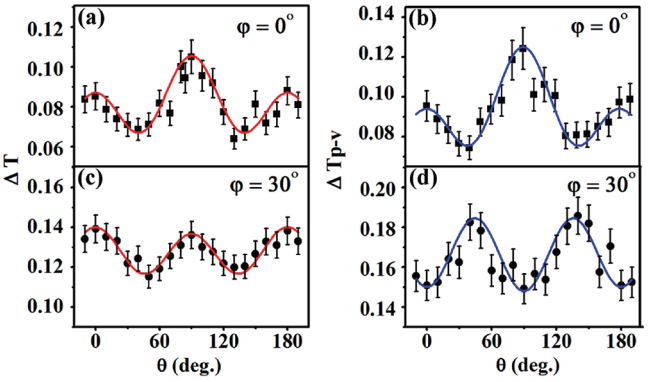

Figure 4. The absolute value of $\Delta T/T$ and the peak to valley change of transmittance, $\Delta T/T_{\text{P-V}}$, as a function of the polarization angle θ, with the sample orientation angle set to 0° for (a) and (b), and 30° for (c) and (d), respectively. The solid line indicates the theoretical fit.

the crystal graphic xz plane is given by $E = E_0(\cos\theta\, z + \sin\theta\, x)$. Since ZnO exhibits a hexagonal structure, the intrinsic permutation symmetry leaves eight independent tensor components. Note that this is true for both TPA coefficient and NLR index. For this specific geometry, the effect third-order susceptibility from eq 5 is

$$\chi^{(3)}_{\text{eff}}(\theta) = \chi^{(3)}_{zzzz}\cos^4\theta + \chi^{(3)}_{xxxx}\sin^4\theta + B\frac{\sin^2 2\theta}{4} \quad (8)$$

where $B = 2\chi^{(3)}_{zxxx} + 2\chi^{(3)}_{xxzz} + 2\chi^{(3)}_{zxxz} + 2\chi^{(3)}_{xzzx}$.

As it is shown in Figure 4a,b, both curves exhibit oscillations with a period of $\pi/2$, which is ascribed to the symmetry of the XZ plane of the single ZnO crystal as indicated in eq 6. Furthermore, the maximum values of $|\Delta T/T|$ and $|\Delta T/T|_{\text{P-V}}$ occur at $\theta = 90°$, in which case $\chi^{(3)}_{xxxx}$ is probed. The largest polarization ratio is obtained that the minimum values of $|\Delta T/T|$ ($\theta = 40°$) and $|\Delta T/T|_{\text{P-V}}$ ($\theta = 40°$) are about 62 and 60% of the maximum values of the $|\Delta T/T|$ and $|\Delta T/T|_{\text{P-V}}$ at $\theta = 90°$, respectively. For the specific direction when polarization angle is 0°, $\chi^{(3)}_{zzzz}$ is excited according to eq 8. Since $|\Delta T/T|$ and $|\Delta T/T|_{\text{P-V}}$ in Figure 4a,b are of a nearly the same polarization dependence, it is obtained that $\chi^{(3)}_{xxxx}/\chi^{(3)}_{zzzz} \approx 1.25$.

Figure 4c,d show the $|\Delta T/T|$ and $|\Delta T/T|_{\text{P-V}}$ as a function of θ at the sample orientation angle $\varphi = 30°$. In this situation, $\mathbf{k}$ propagates parallel to the $[10\bar{1}0]$ direction and the electric-field polarization direction is relative to the c-axis. Because of the isotropy in the crystal graphic XY plane discussed in Figure 3b, it can also be fitted well in eq 8. As it is shown in Figure 4c,d, the curves of $|\Delta T/T|(\theta)$ and $|\Delta T/T|(\theta)$ exhibit an oscillation with a period of $\pi/2$ that is similar to that in Figure 4a,b. The maximum value of $|\Delta T/T|(\theta)$ occurs when the polarization angle is 0° in which case $\chi^{(3)}_{zzzz}$ is probed. The largest polarization ratios are obtained that the minimum value of $|\Delta T/T|(\theta = 45°)$ is about 83% of the maximum value of the $|\Delta T/T|(\theta = 0°)$. Moreover, the curve of $|\Delta T/T|(\theta)$ in Figure 4d exhibits a similar oscillation curve but a phase shift of $\pi/2$ in respect to the curve of $|\Delta T/T|(\theta)$ shown in Figure 4c. Although the minimum and maximum values of $|\Delta T/T|_{\text{PV}}(\theta)$ occur at $\theta = 0$ and 45° shown in Figure 4d, this is opposite to the curve of $|\Delta T/T|(\theta)$, the polarization ratio is determined to be ~81%, which is in good agreement with the results in Figure 4c. The phase shift of $\pi/2$ is attributed to the sign reversal of NLR n_2 from positive to negative (see Supporting Information, Figure S3).

In order to study the size-dependent optical properties, the polarized-related nonlinearities of ZnO micro/nanowires with different diameters, as well as a-plane and c-plane single crystalline bulk ZnO crystal (size: 10 mm × 5 mm × 0.3 mm), were measured in the same method where φ was set as 30°. It is interesting to find that the c-plane ZnO crystal shows no anisotropy nonlinearities (see Supporting Information Figure S4). Figure 5a shows the normalized change in transmittance ($|\Delta T/T|$) as a function of the polarization angle θ (with the sample orientation of 30°) for the ZnO micro/nanowires with diameters of ~120 nm (red curve), ~500 nm (green curve), and ~2.6 μm (blue curve), as well as a-plane ZnO crystal (black curve), respectively. All of the curves exhibit an oscillation with a period of $\pi/2$. Specifically, for the a-plane ZnO crystal, the value of the normalized $|\Delta T/T|(\theta)$ at 0° is significantly larger than that at 90°. As the diameter of the micro/nanowire decreases, the components of the nonlinear response with a vertical polarization direction ($\theta = 90°$) increase significantly. The ratio of the component at $\theta = 90°$ and the component at $\theta = 0°$ ($\beta_{90°}/\beta_{0°}$) as a function of the diameters are presented in Figure 5b (blue curve). It shows that $\beta_{90°}/\beta_{0°}$ increases from 0.67 to 1.08 as the diameters decrease. This important process can be the characteristic of one-dimensional growth of the ZnO micro/nanowire that these highly size-related anisotropies shown in Figure 5a are attributed to the size-confinement effect only in the direction that is vertical to the c-axis of the ZnO micro/nanowire. It is well-known that the size-confinement in nanostructures can result in a deviation of the electronic excitation from a most ideal harmonic oscillator in the bulk crystal, which leads to a large optical enhancement in the nanostructures.[35,36] Thus, the anisotropies of the individual ZnO micro/nanowire in our experiment can be attributed to the contribution of the anisotropy of the third-order

dx.doi.org/10.1021/nl203884j | Nano Lett. XXXX, XXX, XXX−XXX

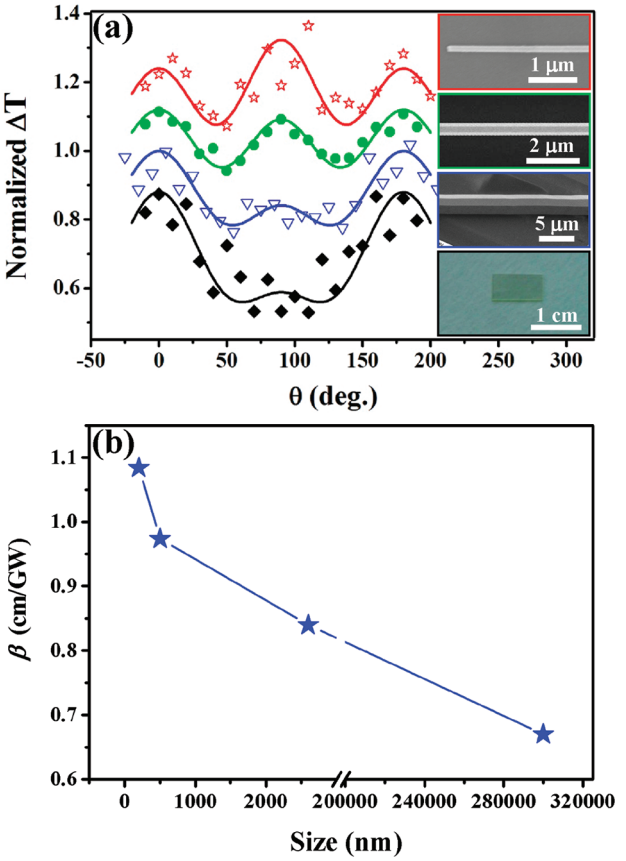

Figure 5. (a) The normalized $\Delta T/T$ as a function of the polarization angle θ, with the sample orientation angle set to 30° in the ZnO micro/nanowires with diameters of ~120 nm (red curve), ~500 nm (green curve), and ~2.6 μm (blue curve), as well as *a*-plane single crystalline ZnO crystal (black curve), respectively. The solid lines indicate the theoretical fit. Insets are the corresponding SEM and optical images of the ZnO micro/nanowires and crystal. (b) The ratios of the component of TPA at $\theta = 90°$ and the component at $\theta = 0°$ as a function of sizes.

nonlinearity of the single crystal lattice and the contribution of the size-confinement effect in the direction that is vertical to the *c*-axis.

According to our study, in the view of nanolaser pumping by TPA effect both parameters of the size of the ZnO micro/nanowire and the polarized angle should be taken into account. Above all, for the ZnO micro/nanowire with a size of 500 nm, the value of the components of $\chi^{(3)}_{zzzz}$ and $\chi^{(3)}_{xxxx}$ are comparable. For the ZnO micro/nanowire with a relatively larger diameter (>500 nm), the polarization direction should keep parallel to the *c*-axis to excite the component of $\chi^{(3)}_{zzzz}$. For the smaller ZnO micro/nanowire (<500 nm), the polarized angle should be set to be 90° in order to excite the larger component of $\chi^{(3)}_{xxxx}$.

In summary, the anisotropic third-order optical nonlinearity of individual ZnO micro/nanowires on the quartz substrate was characterized using Z-scan method with a femtosecond laser. The oscillation patterns of both two-photon absorption and nonlinear refraction as a function of the polarization angle and sample orientation angle were observed. It exhibits a large relative min-max ratio for both parameters, implying a large polarization effect of the individual ZnO micro/nanowire. Furthermore, the size-dependent optical nonlinearity of the ZnO micro/nanowire was observed. These highly size-dependent anisotropies of the third-order nonlinearity in an individual ZnO micro/nanowire has great potential in applications of nanolasers, all-optical switching and high-resolution photodetectors.

■ ASSOCIATED CONTENT

Supporting Information

The low-magnification SEM image of single ZnO nanowire on the quartz substrate; the Raman spectrum of a single ZnO nanowire; the $\Delta T/T$ under different laser intensities; the curves of the difference of the peak and valley of $|\Delta T/T|_{P-V}$ at $\varphi = 0°$ and $\varphi = 30°$, respectively; the change in transmittance ($\Delta T/T$) as a function of the polarization angle, θ, in the *c*-plane single crystalline ZnO crystal. This material is available free of charge via the Internet at http://pubs.acs.org.

■ AUTHOR INFORMATION

Corresponding Author

*E-mail: (J.Z.) jun.zhou@mail.hust.edu.cn; (P.X.L.) lupeixiang@mail.hust.edu.cn; (Z.L.W.) zhong.wang@mse.gatech.edu.

■ ACKNOWLEDGMENTS

This work is supported by National Natural Science Foundation of China (60925021, 51002056 and 51072236), a Foundation for the Author of National Excellent Doctroal Dissertation of PR China (201035), and the Program for New Century Excellent Talents in University (NCET-10-0397). The authors thank the Analysis and Testing Center of Huazhong University of Science and Technology for support.

■ REFERENCES

(1) Cotter, D.; Manning, R. J.; Blow, K. J.; Rogers, D. C. *Science* **1999**, *286*, 1523.
(2) Liu, X. P.; Osgood, R. M.; Vlasov, Y. A.; Green, W. M. J. *Nat. Photonics* **2010**, *4*, 557.
(3) Corcoran, B.; Monat, C.; O'Faolain, L.; Krauss, T. F. *Nat. Photonics* **2010**, *3*, 206.
(4) Leuthold, J.; Koos, C.; Freude, W. *Nat. Photonics* **2010**, *4*, 535.
(5) Foster, M. A.; Turner, A. C.; Lipson, M.; Gaeta, A. L. *Nature* **2006**, *441*, 960.
(6) Huang, M. H.; Mao, S.; Feick, H.; Yang, P. D. *Science* **2001**, *292*, 1897.
(7) Riggs, J. E.; Walker, D. B.; Sun, Y. P. *J. Phys. Chem. B* **2000**, *104*, 7071.
(8) Tatsuura, S.; Furuki, M.; Tian, M.; Mitsu, H. *Adv. Mater.* **2003**, *15*, 534.
(9) Zhu, Y. W.; Elim, H. I.; Foo, Y. L.; Sow, C. H. *Adv. Mater.* **2006**, *18*, 587.
(10) Larson, D. R.; Zipfel, W. R.; Williams, R. M.; Webb, W. W. *Science* **2003**, *300*, 1434.
(11) Dubertret, B.; Skourides, P.; Norris, D. J.; Libchaber, A. *Science* **2002**, *298*, 1759.
(12) Chelnokov, E. V.; Bityurin, N.; Marine, W. *Appl. Phys. Lett.* **2006**, *89*, 171119.
(13) Zhou, H.; Wissinger, M.; Fallert, J.; Kalt, H. *Appl. Phys. Lett.* **2007**, *91*, 181112.
(14) Zhang, C. F.; Dong, Z. W.; Qian, S. X. *Opt. Lett.* **2006**, *31*, 3345.
(15) Zhang, C.; Zhang, F.; Xia, T.; Xu, J. *Opt. Exp.* **2009**, *17*, 7893.
(16) Wang, J. F.; Gudiksen, M. S.; Duan, X. F.; Lieber, C. M. *Science* **2001**, *293*, 1455.
(17) DeSalvo, R.; Sheik-Bahae, M.; Stryland, E. W. *Opt. Lett.* **1993**, *18*, 194.
(18) Neumann, U.; Grunwald, R.; Griebner, U.; Seeber, W. *Appl. Phys. Lett.* **2005**, *87*, 171108.
(19) Hurlbut, W. C.; Lee, Y. S.; Fejer, M. M. *Opt. Lett.* **2007**, *32*, 668.
(20) Zhang, J.; Lin, Q.; Fauchet, P. M. *Appl. Phys. Lett.* **2007**, *91*, 071113.

dx.doi.org/10.1021/nl203884j | *Nano Lett.* XXXX, XXX, XXX−XXX

(21) Ganany-Padowicz, A.; Juwiler, I.; Gayer, O.; Arie, A. *Appl. Phys. Lett.* **2009**, *94*, 091108.
(22) Pan, Z. W.; Dai, Z. R.; Wang, Z. L. *Science* **2001**, *291*, 1947.
(23) Wang, Z. L; Song, J. H. *Science* **2006**, *312*, 242.
(24) Huang, M.; Mao, S.; Feick, H.; Yan, H.; Wu, Y.; Kind, H.; Weber, E.; Russo, R.; Yang, P. *Science* **2001**, *292*, 1897.
(25) Johnson, J. C.; Yan, H. Q.; Schaller, R. D.; Saykally, R. J. *Nano Lett.* **2002**, *2*, 279.
(26) Chien, C. T.; Wu, M. C.; Chen, C. W.; Chen, Y. F. *Appl. Phys. Lett.* **2008**, *92*, 223102.
(27) Sheik-Bahae, M.; Said, A. A.; Wei, T. H.; Van Stryland, E. W. *IEEE J. Quantum Electron.* **1990**, *26*, 760.
(28) Zhou, J.; Gu, Y. D.; Fei, P.; Mai, W. J.; Gao, Y. F.; Yang, R. S.; Bao, G.; Wang, Z. L. *Nano Lett.* **2008**, *8*, 3035.
(29) Zhou, J.; Fei, P.; Gu, Y. D.; Mai, W. J.; Gao, Y. F.; Yang, R. S.; Bao, G.; Wang, Z. L *Nano Lett.* **2008**, *8*, 3973.
(30) Zhou, J.; Fei, P.; Gao, Y. F.; Gu, Y. D.; Bao, G.; Wang, Z. L. *Nano Lett.* **2008**, *8*, 2725.
(31) Zhou, J.; Gu, Y. D.; Hu, Y. F.; Mai, W. J.; Yeh, P. H.; Bao, G.; Sood, A. K.; Polla, D. L.; Wang, Z. L. *Appl. Phys. Lett.* **2009**, *94*, 191103.
(32) Calleja, J. M.; Cardona, M. *Phys. Rev. B* **1977**, *16*, 3753.
(33) Arbouet, A.; Christofilos, D.; Fatti, N. D.; Vallée, F. *Phys. Rev. Lett.* **2004**, *93*, 127401.
(34) Carey, C. R.; LeBel, T.; Crisostomo, D.; Giblin, J.; Kuno, M.; Hartland, G. V. *J. Phys. Chem. C* **2010**, *114*, 16029.
(35) Hanamura, E. *Phys. Rev. B* **1988**, *37*, 1273.
(36) Lee, H. W.; Lee, K. M.; Lee, S.; Koh, K. H.; Park, J. Y.; Kim, K.; Rotermund, F. *Chem. Phys. Lett.* **2007**, *447*, 86.

dx.doi.org/10.1021/nl203884j | *Nano Lett.* XXXX, XXX, XXX−XXX